# Perovskite Photovoltaic Integrated CdS/$TiO_2$ Photoanode for Unbiased Photoelectrochemical Hydrogen Generation

Siva Krishna Karuturi,[1*†] Heping Shen,[2*†] The Duong,[2] Parvathala Reddy Narangari,[1] Rowena Yew,[1] Jennifer Wong-Leung,[1] Kylie Catchpole,[2] Hark Hoe Tan,[1] Chennupati Jagadish[1]

1. Department of Electronic Materials Engineering, Research School of Physics and Engineering, Australian National University, Canberra , ACT 2601 , Australia
2. Research School of Engineering, Australian National University, Canberra, ACT 2601, Australia

[†]These authors contributed equally to this work.

[*] Corresponding authors: siva.karuturi@anu.edu.au; heping.shen@anu.edu.au

## ABSTRACT

Photoelectrolysis of water using solar energy into storable and environmental-friendly chemical fuel in the form of hydrogen provides a potential solution to address the environmental concerns and fulfil future energy requirements in a sustainable approach. Achieving efficient and spontaneous hydrogen evolution in water using solar light as the only energy input is a highly desirable but a difficult target. In this work, we report perovskite solar cell integrated CdS based photoanode for unbiased photoelectrochemical hydrogen evolution. An integrated tandem device consisting of mesoporous CdS/$TiO_2$ photoanode paired with a triple-cation perovskite ($Cs_{0.05}(MA_{0.17}FA_{0.83})_{0.95}Pb(I_{0.83}Br_{0.17})_3$) solar cell is developed using a facile fabrication route. The proposed PV integrated photoanode presents an efficient tandem configuration with high optical transparency to long wavelength photons and strong photoelectrochemical conversions from short wavelength photons. Based on this integrated tandem device, an unbiased photocurrent density of 7.8 mA/$cm^2$ is demonstrated under AM1.5G illumination.

**KEYWORDS:** Photoelectrochemical, Perovskite Solar Cell, Hydrogen Generation, Tandem Semiconductors, Atomic Layer Deposition

## INTRODUCTION

With rising concerns from ever increasing global energy demand and environmental sustainability, development of new energy technologies with least impact on the environment is critical to the continuation of socio-economic development. With 120 000 terawatts (TW) of light energy striking the earth's surface at any given instant, solar energy is by far the most abundant clean energy resource accessible . While stand-alone photovoltaic cells are proven to generate electricity cheaply, transportable fuels are still critical in a carbon-constrained world.[1-2] An elegant and potentially low cost route to storing solar energy is to convert the sun energy directly into a storable chemical fuel such as hydrogen, similar to the photosynthesis process utilized by nature. Since the product of hydrogen combustion is water, it is a clean transportable fuel.[3-4] Ever since the first report of sunlight induced hydrogen generation using $TiO_2$ four decades ago, photoelectrochemical (PEC) water splitting has been intensely investigated using various semiconductor photoelectrodes.[5-8] However, the main requirement for a photoelectrode in a PEC cell to induce spontaneous hydrogen evolution is the availability of a semiconductor with an appropriate bandgap of ~2.5 eV, having a conduction band and valence bands straddling the water redox potentials. Unfortunately, devices capable of spontaneous gas evolution are inefficient because the photoelectrodes with a bandgap of around 2.5 eV absorb only a small portion of the solar spectrum.[9-12]

One approach to solve this problem of single semiconductor photoelectrodes is the use of a tandem semiconductor systems.[10, 12-14] By relaxing the constraint that only a single semiconductor material can be used, a combination of semiconductors with complementary bandgaps can be employed.[9] This permits simultaneously building up sufficient voltage to induce spontaneous water splitting reaction, and utilizing a larger proportion of solar spectrum, enabling high STH efficiencies. PEC systems delivering STH efficiency up to 14% have been demonstrated with this approach using III-V tandem structures, but these materials are very expensive for practical applications.[10, 11] Also, the stability of these systems has reached only up to tens of hours. It is a difficult task to develop two semiconductor photoelectrodes with appropriate bandgaps with sufficient operational stability in the same electrolyte for both anodic and cathodic operations, respectively. One approach to solve this problem of stability is the use of a photovoltaic-photoelectrochemical (PV-PEC) configuration, also called PV biased PEC systems (see Fig. 1).[12] A photoelectrode combined with an appropriate PV cell with complimentary absorption ability can harvest a wide region of the solar spectrum and produce high solar to hydrogen conversion efficiency. Achieving this potential requires the development of a photoelectrode with good light absorption, photoelectrochemical performance, and stability using raw materials of ample availability. This photoelectrode then needs to be integrated with an appropriate low-cost photovoltaic (PV) cell with complementary absorption ability and a counter electrode (anode) with high catalytic efficiency and stable performance.

A range of PV cells including silicon, perovskite and dye sensitized solar cells have been investigated as a means of supplying additional bias to achieve overall water splitting without the need for external electricity input.[14-21] Impressive solar-to-hydrogen conversion efficiencies that were not previously possible with single semiconductor PEC approach have been reported in the last few years. Among different PV devices, solution-processed perovskite cells provide ultimate opportunities for solar hydrogen generation, particularly due to their large photovoltages.[22-23] In addition to the low-cost solution processing and high PV performance,

perovskites cells also offer advantages such as bandgap tunability and optical transparency, enabling their application as both top and bottom absorber in tandem configurations.[24] So far, perovskite PVs have been studied for solar water splitting in PV-PEC configuration using photoelectrodes made of hematite,[14] $BiVO_4$,[19-21, 25-26] $Cu_2O$[27] and CIGS[18]. A highest unbiased photocurrent density 5.12 $mA/cm^2$ corresponding to solar-to-hydrogen efficiency of 6.3% has been demonstrated when it is employed in tandem with either $BiVO_4$ photoanode or CIGS photocathode.[18, 21]

Herein, we report a perovskite PV integrated CdS photoanode for spontaneous hydrogen evolution using a facile fabrication route. A combination of solution processing and atomic layer deposition techniques are used to fabricate the integrated device on a double-side conducting, transparent glass. The proposed integrated device satisfies all the critical requirements of an efficient tandem configuration such as complementary light absorption with high optical transparency to long wavelength photons and strong photoelectrochemical conversion from short wavelength photons. A highest photocurrent density of 7.8 $mA/cm^2$ is realized at 0 V bias condition for spontaneous hydrogen evolution under AM1.5 G illumination.

## RESULTS & DISCUSSION

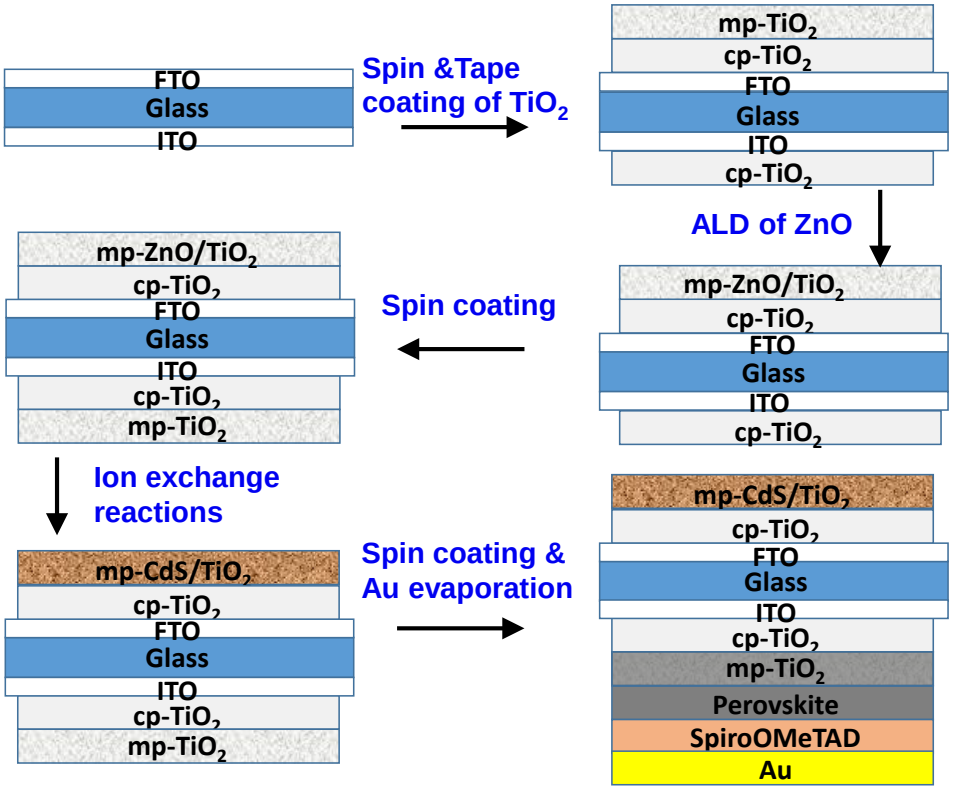


**Figure 1.** Schematic illustration of the fabrication of Perovskite-CdS/$TiO_2$ integrated PV-PEC device.

The fabrication procedure for the integrated PV-PEC tandem device consisting of a CdS/$TiO_2$ photoanode as a top absorber and an encapsulated perovskite PV as a bottom absorber is schematically illustrated in Figure 1. A double-side conductive substrate is specifically designed for this work for constructing the integrated tandem device. We used commercial FTO-coated substrate and sputtered ITO on the opposite side of the glass to achieve double side conducting properties with optimum transparency. The double side conducting glass

substrate is first spin coated with a 50 nm of compact-$TiO_2$ (cp-$TiO_2$) film on both sides. After annealing the glass substrate at 500 $^oC$, a mesoporous-$TiO_2$ (mp-$TiO_2$) film is tape casted on the FTO side. A sacrificial ZnO film of desired thickness is deposited conformally in the mp-$TiO_2$ film using atomic layer deposition (ALD) in high aspect ratio deposition method.[28] During the ZnO deposition, the substrate was covered around the edges with a Kapton tape to prevent any unwanted deposition occurring on the rear surface. Next, ~120 nm of mp-$TiO_2$ film is spin coated on the ITO side. The resulting substrate was further annealed at 500 $^oC$ in air. The ZnO ALD film is subsequently converted into CdS via ion exchange reactions.[29] Compared to the conventional dip coating and physical deposition techniques used for CdS deposition,[30-32] the ALD and ion exchange methods used in this work selectivity deposit CdS conformally in the mp-$TiO_2$ on the FTO side of the glass without interfering with the fabrication of perovskite PV on the ITO side of the substrate. Also, possible air annealing of CdS which could result in oxidation of CdS is eliminated by carrying out the air annealing steps before the ion exchange reactions. Next, the fabrication of perovskite PV on the ITO side of the substrate is carried out as reported in our previous work.[33] Detailed experimental procedure can be found in the experimental section. We note that the perovskite PV is encapsulated for protecting the device from water degradation. An innovative “double-sealing method” is developed in which the device is first encapsulated with a thin glass slide using hot-melting Surlyn and then followed by edge sealing using epoxy with UV treatment.

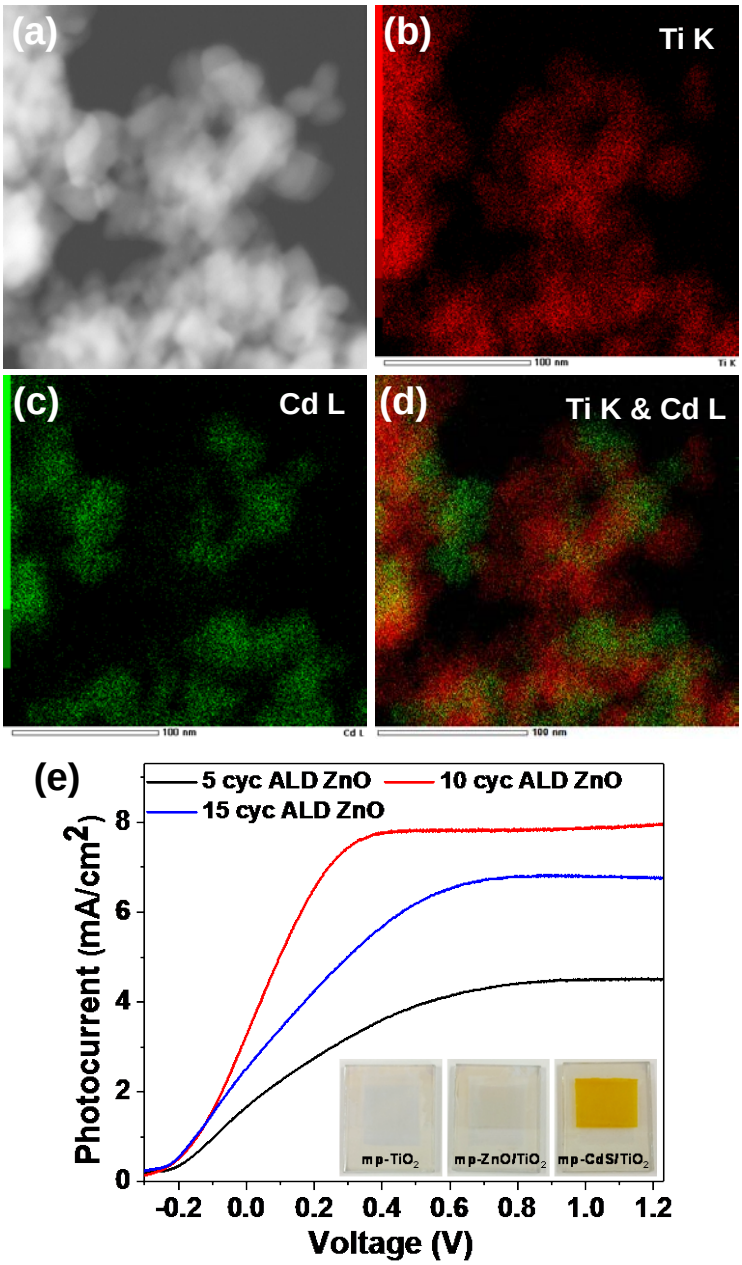


**Figure 2.** (a) High angle annular dark field STEM image and corresponding STEM-EDX maps of (b) Ti K (c) Cd L, (d) Ti K (red) & Cd L (green) overlapped of mp-CdS/$TiO_2$ and (e) Linear sweep voltammetry measurements of mp-CdS/$TiO_2$ photoanode based on different thicknesses of ALD ZnO sacrificial film in 0.25 M $Na_2S$ and 0.35 M $Na_2SO_3$ electrolyte. The inset shows the photographs of the photoanode at different stages of fabrication.

To determine the optimum coating of CdS on mp-$TiO_2$, sacrificial ZnO films of varying thickness were deposited using ALD. The growth rate of ZnO was found to be 0.15 nm per cycle based on ellipsometry measurements on silicon wafer. We observed exfoliation of the mesoporous films with ZnO film depositions above 15 ALD cycles (~2.25 nm) after ion exchange reactions. This could be due to the volume expansion of the films after ion exchange process as the ionic radii of Cd and S are significantly higher than that of Zn and O, respectively. CdS obtained through ion exchange reactions of ZnO is found to be in hexagonal crystal phase from X-ray diffraction analysis (Figure S1). It is well known that ALD deposits films conformally on high aspect ratio substrates.[34-35] However, CdS obtained though ion

exchange reactions of ZnO ALD film is found to be nonconformal in STEM-EDX elemental mapping (Figure 2). This could be due to the aggregation of CdS into nanocrystal morphology after ion exchange and annealing. Luo *et al.*, also found that CdSe obtained from sacrificial ZnO ALD films through ion exchange process presents nanocrystal morphology.[29] Photoelectrochemical performance of the as-obtained mp-CdS/$TiO_2$ photoanodes of different CdS thickness were evaluated in a three electrode setup. Figure 2 shows the current-voltage characteristics of the CdS photoanodes based on different ZnO films thicknesses. All the photoanodes present similar onset potential. A highest saturated photocurrent of ~ 7.8 mA/cm$^2$ was obtained from the photoanode based on 10 cycles of sacrificial ZnO film. This is one of the best reported photocurrents for CdS based photoelectrodes.[36] The combination of ALD and ion exchange reactions used in this work helps in achieving this performance by addressing the issues of pore clogging and non-uniform coating that are generally associated with the conventional dip coating or line-of-sight physical deposition methods.

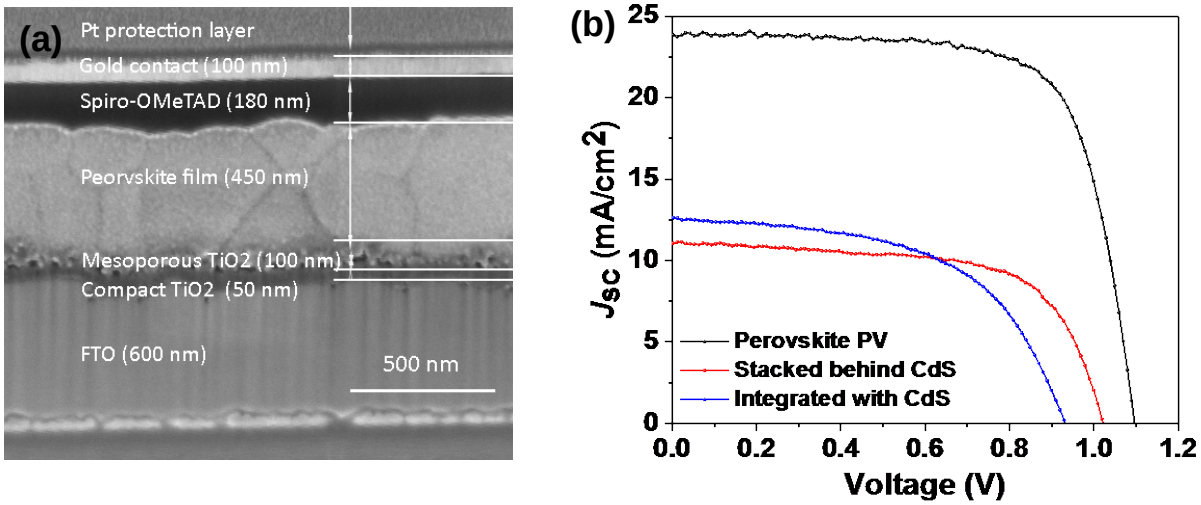


**Figure 3. (**a) Cross-sectional scanning electron microscopy (SEM) image of the perovskite solar cell. (b) Illuminated *J-V* curves of the perovskite PV based on triple-cation perovskite ($Cs_{0.05}(MA_{0.17}FA_{0.83})_{0.95}Pb(I_{0.83}Br_{0.17})_3$) film measured in standalone, stacked and integrated configurations.

Perovskite PV used in this work presents an n-i-p mesoporous structure including FTO/cp-$TiO_2$/mp-$TiO_2$/perovskite/Spiro-OMeTAD (2,2',7,7'-Tetraakis-(N,N-di-4-methoxyphenylamino)-9,9'-spirobifluorene)/gold. From its cross-sectional SEM image (Fig. 3a), the compact $TiO_2$ is ~50 nm, and the mesoporous $TiO_2$ layer has a thickness of ~120 nm. Triple-cation (cesium (Cs)/formamidinium (FA)/methylammonium (MA)) perovskite with a composition of $Cs_{0.05}(MA_{0.17}FA_{0.83})_{0.95}Pb(I_{0.83}Br_{0.17})_3$ and a corresponding bandgap of ~1.6 eV is used in this work instead of the widely used $MAPbI_3$, as it has been proven to show improved stability, reproducibility and high efficiency.[37] The perovskite film thickness was controlled at ~450 nm, which enables sufficient light absorption in the visible region. The hole transport layer Spiro-OMeTAD is ~130 nm thick, covered by a ~100 nm gold contact layer. The top Pt layer has been deposited as a protection layer from ion beam milling of the sample for cross-sectional imaging. Perovskite standalone device was first fabricated to assess the photovoltaic performance of the perovskite PV. The standalone PV cell showed a slight hysteresis behavior (Fig. S3), which has been widely reported in the mesoporous structure and can be alleviated by further improving the perovskite and interface qualities.[38-39] From the reverse *J-V* scanning curve, the perovskite PV exhibits an efficiency of ~18.8%, attributed by an open-circuit voltage

($V_{oc}$) of 1.095 V, short-circuit current ($J_{sc}$) of 23.8 mAcm$^{-2}$, and FF of 0.72. In a mechanically-stacked configuration, it retains a $J_{sc}$ of ~10.4 mAcm$^{-2}$ after filtering of short wavelength photons by a CdS photoanode, coupled with a $V_{oc}$ drop of ~80 mV. In the integrated structure, the $V_{oc}$ and FF yield are slightly inferior due to the increased complexity in device fabrication. Nevertheless, the integrated PV/PEC structure shows a prominently increased current yield of ~12.7 mAcm$^{-2}$, due to less parasitic absorption (only one substrate is involved) and reduced reflection losses, which will be further analyzed in the next section. The effectiveness of the "double-sealing method" for encapsulating the perovskite solar cell (PSC) to survive in water has been proven by testing the photovoltaic performance degradation over several days confirming excellent sealing of the cell (Fig. S4).

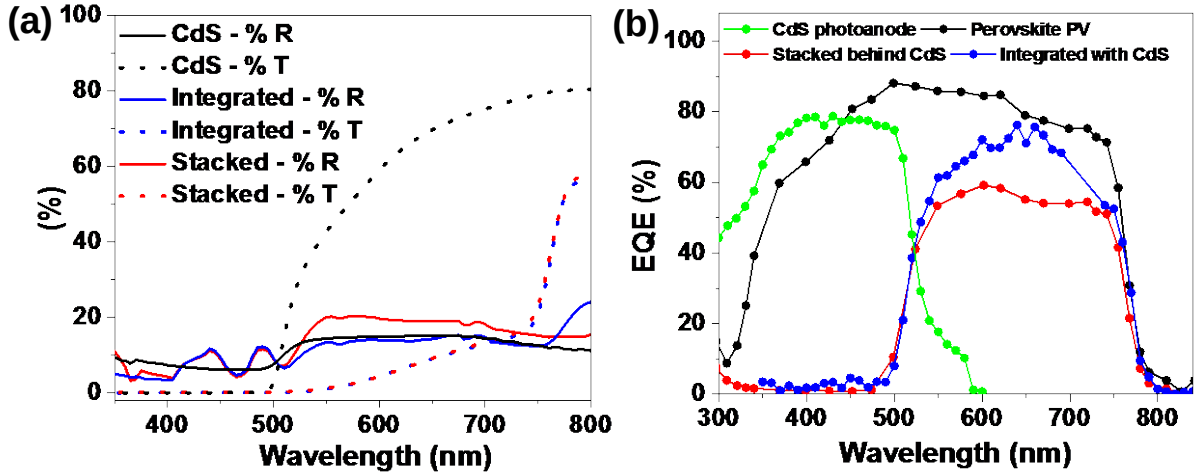


**Figure 4.** (a) Transmittance and reflectance spectra, (b) wavelength dependent quantum efficiency of CdS photoanode, perovskite PV stacked behind CdS photoanode and perovskite PV integrated with CdS photoanode.

Transmittance and reflectance characteristics of CdS photoanode and perovskite PV paired with CdS in both the stacked and integrated configurations are shown in Figure 4a. From the transmittance spectrum of CdS photoanode, it can be seen that the mp-CdS/$TiO_2$ is highly transparent to the sub-bandgap photons, allowing efficient absorption of lower energy photons by the bottom perovskite PV. It is noted that mp-$TiO_2$ is a highly suitable host structure for CdS compared to higher dimensional nanostructures such as nanowires or inverse opals as they present significant scattering resulting in inefficient transmission of sub-bandgap photons. There is no observable difference between the transmittance of the paired devices in both the stacked and integrated configurations. However, the integrated structures shows reduced reflectance in the wavelength range of 500 to 800 nm which is beneficial for enhanced light harvesting by the bottom PV. The airgap between the two substrates in the stacked configuration contributes to the additional reflection losses. Moreover, the integrated configuration also minimises the additional transmission losses occurring from the double glass substrates used in the stacked configuration. Figure 4b shows the wavelength dependent current conversion efficiency of the CdS photoanode and perovskite PV. CdS photoanode presents excellent incident photon-to-electron conversion efficiency (IPCE) of high energy photons below 500 nm, which is an important attribute of a top absorber in an efficient tandem device. Interestingly, CdS exhibited particularly long absorption tail extending up to 600 nm demonstrating significant quantum efficiency in this wavelength region. This anomaly resulting in lowering of effective bandgap has been shown and discussed in various previous

works.[8, 40] Though the reason for the absorption tail extension is still widely debated, non-stoichiometry and the presence of intermediate states are attributed as possible explanations. Similarly, the bottom perovskite PV presents excellent complimentary light harvesting ability with high external quantum efficiency (EQE) for low energy photons in the wavelength range of 500 to 750 nm. Meanwhile, there is an observable difference between the EQE of the perovskite PV in the stacked and integrated configurations. Perovskite PV in the integrated configuration presents higher EQE in consistence with its reflectance and *J-V* characteristics.

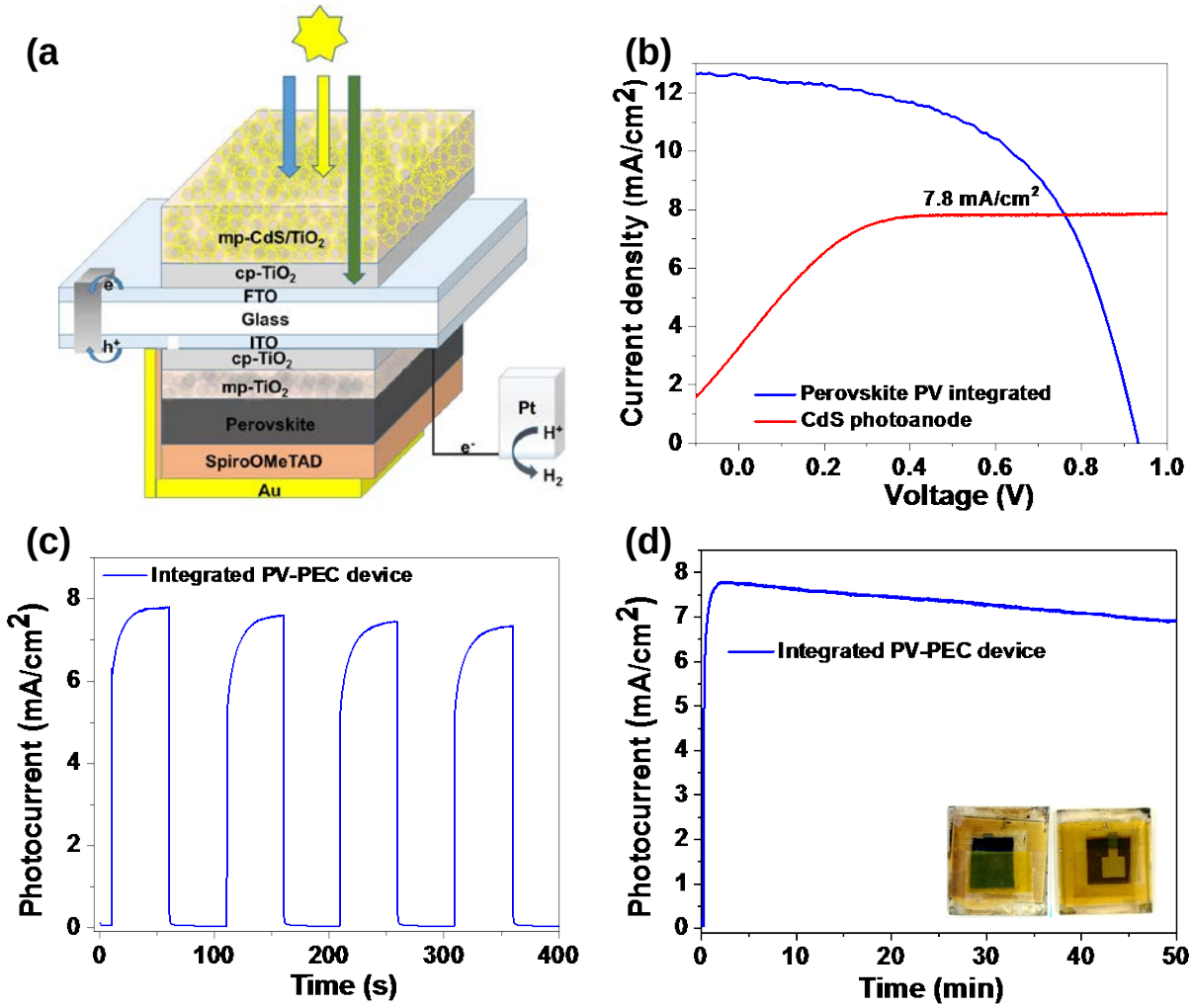


**Figure 5. (**a) Schematic of integrated PV-PEC device for solar hydrogen generation. (b) TEM characterization of CdS/mp-$TiO_2$. b. *J-V* curve of CdS photoanode overlaid with the *J-V* response of the perovskite PV. PEC performance of CdS/mp-$TiO_2$ photoanode based on different thicknesses of ZnO sacrificial film. Chronoamperometry *J-t* curves for the PV integrated photoanode at an applied potential of 0 V with 50 s light on/off cycles (c) and 50 mins of continuous illumination (d). The inset shows the photographs of the integrated device taken on both sides.

The working mechanism of the PV-PEC device in the integrated configuration for spontaneous solar hydrogen generation is schematically illustrated in Figure 5a. Operating point of the integrated device can be determined by overlaying the *J-V* curves of CdS photoanode and perovskite PV in the integrated structure. As shown in Figure 5b, a photocurrent density of 7.8 mA/$cm^2$ for spontaneous hydrogen evolution is realized at the intersection point of 0.76 V. This is the highest reported value for the perovskite PV integrated photoelectrodes. It is noteworthy that the photovoltage generated by the bottom light absorber at the operating current condition is much in excess to the minimum requirement. Considering sulfide oxidation

at CdS photoanode, the excess voltage will provide any additional voltage losses that may occur for overall water splitting. Figure 5c presents the photocurrent vs. time curve of the integrated device without any bias under chopped simulated AM 1.5G illumination during the initial 400 s. Slightly sluggish photoresponse during light on/off cycles is expected to be caused by the relatively slow transient response of perovskite PV, usually in a timescale of tens of seconds [41-42]. Such a slow transient behavior has been widely reported and has been attributed to a few factors including the ion migration and defects filling.[38] The long term photostability characteristics of the integrated device presented in Figure 5d shows that the photocurrent gradually decreases with time. This is likely due to photocorrosion of CdS since the perovskite PV presents relatively stable performance when encapsulated. We anticipate that the addition of co-catalyst such as Co-Pi and IrOx may resolve the issue of stability for CdS and further work is greatly needed in this direction.[43-44] Kim *et al.,* demonstrated the only perovskite PV integrated photoelectrode by pairing $CH_3NH_3PbI_3$ perovskite solar cell with $BiVO_4$ photoanode demonstrating an unbiased photocurrent of 4.05 mA/cm$^2$ and STH efficiency of ~5 %.[19] With the highest unbiased photocurrent of 7.8 mA/cm$^2$ realized in this work based on the integrated structure, we believe that addressing the stability of CdS for overall water splitting holds the key towards the accomplishment of artificial leaf type of water splitting device with STH efficiencies above 10 % via low cost approaches.

## CONCLUSIONS

In this work, we have developed a PV integrated photoanode for spontaneous solar hydrogen generation by pairing a triple-cation perovskite PV and a CdS photoanode for the first time. Stability of the perovskite PV in water is achieved through encapsulation using a double-sealing method. CdS is deposited selectively in mesoprous-$TiO_2$ host film using a combination of atomic layer deposition and ion exchange reaction methods. It is found that perovskite bottom absorber provides photovoltage much in excess of the requirement to generate a photocurrent of 7.8 mA/cm$^2$ at 0 V applied bias for spontaneous hydrogen evolution. The integrated device also showed superior optical and light harvesting performance in comparison to the stacked tandem device. The integrated device reported in this work shows promise for the development of artificial leaf type of wireless solar water splitting devices with above 10 % solar-to-hydrogen conversion efficiencies. The reported integrated device also presents opportunities for tandem PVs based on perovskite and quantum dot solar cells.

## EXPERIMENTAL SECTION

### Materials

All the materials were used as obtained from suppliers without any further purification. Methylammonium iodide (MAI) and mesoporous $TiO_2$ (mp-$TiO_2$) paste (30 NR-D) were purchased from Dyesol. 2,2',7,7'-Tetrakis-(N,N-di-4-methoxyphenylamino)-9,9'-spirobifluorene (Spiro-MeOTAD) powder was purchased from Luminescence Technology. For ion exchange reactions, cadmium acetate dihydrate ($Cd(Ac)_22H_2O$, 98%) and sodium sulfide nonahydrate ($Na_2S$, 99%) were purchased from Alfa Aesar. All the other materials were bought from Sigma Aldrich.

### Fabrication procedures

#### *Deposition of cp-$TiO_2$ and mp-$TiO_2$ films*

2 x 2 cm$^2$ of FTO glass substrates (7Ω/□) were cleaned sequentially with detergent, acetone, isopropyl alcohol (IPA) and ethanol using ultrasonic bath for 15 mins each.

ITO was sputtered on the glass side of the above cleaned substrates using ATC 2400-V sputtering system (AJA International Inc.) with the RF power of 90 W and chamber pressure of 1.5 mTorr for 3600 s at room temperature. The substrates were then annealed at 500 ℃ in air for 1 hour. Final thickness of the sputtered ITO is ~100 nm and the sheet resistance is ~30 Ω/□. It is noted that the ITO film was laser cut to avoid the shortage condition. The as-prepared double-side conductive transparent substrates were then further cleaned with acetone, IPA and ethanol for 15 mins each. Before the usage, they were further treated with oxygen plasma for 30 mins on both sides.

50 nm compact $TiO_2$ films were then deposited on both sides of the substrates using a solution based method. 350 μL Titanium isopropoxide (TTIP) in 2.5 mL anhydrous ethanol was firstly mixed with 35 μL 2 M HCl in 2.5 mL ethanol under continuous stirring for 10 mins. The $TiO_2$ precursor solution was then spin-coated at 2000 rpm/s for 1 min. The substrates were then annealed at 500 ºC for 30 mins in air, and allowed to cool down to room temperature. Next, ~6 μm mp-$TiO_2$ films were coated onto the FTO side using tape-casting method, which serves as a scaffold host for CdS. They were sintered at different temperatures in a multi-step procedure. The sintering furnace temperature was first raised to 325 ºC and maintained at 325 ºC for 5 mins, followed by further raise to 375 ºC and upholding for 5 mins, then to 450 ºC and upholding for 10 mins, and finally raised to 500 ºC with continuous sintering for 30 mins. Conformal ZnO films were then deposited onto the mp-$TiO_2$ films using ALD (Savannah 100) with $H_2O$ and Diethylzinc (DEZ, 99.99%, Sigma Aldrich) as the O and Zn sources, respectively. The other side of the substrate was protected from ALD deposition using Kapton tape. Then, ~120 nm thin mp-$TiO_2$ layer was deposited on the ITO side via spin-coating of mp-$TiO_2$ paste solution for 30 s at 5000 rpm, where the mp-$TiO_2$ paste solution was prepared from 30 nm $TiO_2$ particle paste diluted in anhydrous ethanol (1:6, w/w). After the spin-coating, the samples were annealed at 100 ºC for 10 mins, then sintered at 500 ºC for 30 mins in air, and left to cool down to room temperature.

***Solution ion exchange of ZnO to CdS***

The conformal ZnO films deposited on ~10 μm mp-$TiO_2$ films were subjected to ion exchange reactions involving sulfidation in 0.25M $Na_2S$ solution at 60 ºC for 4 h, and cadmiation in 0.1M cadmium acetate dihydrate $(Cd(Ac)_2 2H_2O$ at 120 ºC for 12 h, to convert ZnO to ZnS and subsequently to CdS, respectively. The composition of the $Zn_xCd_{1-x}S$ can be tuned by controlling the reaction temperature. The samples were then cleaned in deionized water and absolute ethanol, followed by annealing at 400 ºC with Argon flow for 45 minutes to enhance crystallinity. The detailed procedure can also be found in our previous work.[8]

***Perovskite solar cell fabrication***

The triple cation based perovskite precursor solution was prepared by mixing CsI (0.065 M), FAI (1.1 M), $PbI_2$ (1.2 M), MABr (0.2 M) and $PbBr_2$ (0.2 M) in anhydrous DMF:DMSO (4:1, v/v). Perovskite film with the composition of $Cs_{0.05}(MA_{0.17}FA_{0.83})_{0.95}Pb(I_{0.83}Br_{0.17})_3$ was deposited by a two-step spin coating procedure: first at 2000 rpm/s with a ramping speed of 200 rpm/s for 10 s, and then at 6000 rpm/s with a ramping speed of 2000 rpm/s for 20 s. Next, ~100 μl chlorobenzene was dropped on the spinning substrates 10 s after the program start. The films were then annealed on the hotplate at 100 ºC for 30 mins.

Spiro-MeOTAD solution was prepared by dissolving 72.5 mg Spiro-OMeTAD, 28.5 μl 4-tert-butypyridine (TBP) and 17.5 μl of lithium bis(trifluoromethanesulfonyl)imide solution (520

mg/ml in acetonitrile) in 1 mL chlorobenzene. The solution was then spin-coated onto the substrate with a speed of 3000 rpm/s for 30 s. Note that, the devices need to be put in the humidity control box for overnight for oxidizing Spiro-MeOTAD. Finally, Au film was then deposited on the Spiro-MeOTAD layer using thermal evaporation technique with a thickness of 100 nm.

To enable good stability of the devices in the water, encapsulation was carried out for the perovskite solar cells using a two- step process. Firstly, the device was sealed by a thin glass slide with the aid of a 30 μm low temperature thermoplastic sealant (Surlyn, Dysol). The sealant film was melted via soldering. On top of it, another larger glass slide is placed with epoxy (Ossila) inserted between two glasses, which is later cured by an UV light source.

**Characterizations**

The surface morphology of the samples was investigated by a FEI Verios scanning electron microscope (SEM). A Helios Nanolab 600 FIB system was employed to prepare cross-sectional SEM images of the cells, where Pt layers were deposited to protect the cell from the damage resulted by Si ion milling. The optical properties of the samples were measured by a PerkinElmer Lambda 1050 UV/Vis/NIR spectrophotometer. X-ray diffraction (XRD) analysis was carried out usinga Bruker D2 Phaser diffractometer at 30 kV, 10 mA at 2θ (Cu Kα) 10–80°, step 0.02° and scan speed 2.3° $min^{-1}$. Transmission electron microscopy (TEM) characterisations were conducted using a JEOL 2100F operated at 200keV with capabilities for both scanning TEM (STEM) and an electron dispersive X-ray (EDX) detection.

As for the *J-V* measurements of the solar cells, the samples were tested under simulated AM 1.5G 1 sun condition (with 100 mW/$cm^2$ power) at 25 $^oC$ with a solar simulator system (model #SS150 from Photo Emission Tech Inc) equipped with a Xenon lamp. A certified Fraunhofer CalLab reference cell was for light intensity calibrations. A custom-built vacuum measurement jig was used to test the perovskite solar cells without any aperture mask. *I-V* sweeps were evaluated using a potentiostat (Autolab PGSTAT302N), with a scanning rate of 50 mV/s without prebiasing. A modified Protoflex QE1400 system was used to test the external quantum efficiency (EQE) of the perovskite solar cells, without light bias in DC mode using a tungsten light source, two Keithey 2425 source meters, and a Si-reference cell. The EQE spectral response was also calibrated using a certified Fraunhofer CalLab reference cell.

A potentiostat (Autolab, PGSTAT302N) was used to measure photoelectrochemical performance of CdS photoelectrodes in a three-electrode configuration with Ag/AgCl in saturated KCl as a reference and a Pt wire as a counter electrodes. 0.25 M $Na_2S$ and 0.35 M $Na_2SO_3$ mixed aqueous solution was used as a sacrificial electrolyte with a pH of ~12.5. A solar simulator (from Newport) equipped with a 150 W Xe lamp and an AM 1.5G filter, was used to measure the photoresponse characteristics under simulated sun light calibrated with a standard Si solar cell. Photocurrent stability tests were carried out at an applied bias of 0 V versus Ag/AgCl under chopped light illumination (light/dark cycles of 50 s). The incident-photon-to-current conversion efficiency (IPCE) measurements were carried out in three-electrode configuration in the wavelength range of 300 to 800 nm using a 1000W Xe lamp equipped with a monochromator. A standard silicon photodiode was used to calibrate the incident light intensity. The electrode potential versus Ag/AgCl was adapted into the reversible hydrogen electrode (RHE) potential as per the Nernst equation[4]: $E_{RHE} = E_{Ag/AgCl} + 0.059\,pH + E^o_{Ag/AgCl}$, where $E_{RHE}$ is the converted potential

vs. RHE, $E^{o}_{Ag/AgCl}$ = 0.1976 V at 25 °C, and $E_{Ag/AgCl}$ is the measured potential against the Ag/AgCl reference electrode.


## ACKNOWLEDGEMENTS

S K. K acknowledges the financial support from the ARC Discovery Early Career Researcher Award grant (DE150100752). The financial support by Australian government through the Australian Research Council (ARC) and Australian Renewable Energy Agency (ARENA) is greatly acknowledged. Access to the facilities of the Centre for Advanced Microscopy (CAM) and the Australian National Fabrication Facility (ANFF) is gratefully acknowledged.


## REFERENCES


1. Lewis, N. S.; Nocera, D. G., Powering the planet: Chemical Challenges in Solar Energy Utilization. *Proceedings of the National Academy of Sciences* **2006,** *103* (43), 15729-15735.
2. Lewis, N. S., Research Opportunities to Advance Solar Energy Utilization. *Science* **2016,** *351* (6271).
3. Crabtree, G. W.; Dresselhaus, M. S.; Buchanan, M. V., The Hydrogen Economy. *Physics Today* **2004,** *57* (12), 39-44.
4. Kamat, P. V.; Tvrdy, K.; Baker, D. R.; Radich, J. G., Beyond Photovoltaics: Semiconductor Nanoarchitectures for Liquid-Junction Solar Cells. *Chemical Reviews* **2010,** *110* (11), 6664-6688.
5. Walter, M. G.; Warren, E. L.; McKone, J. R.; Boettcher, S. W.; Mi, Q.; Santori, E. A.; Lewis, N. S., Solar Water Splitting Cells. *Chemical Reviews* **2010,** *110* (11), 6446-6473.
6. Gratzel, M., Photoelectrochemical Cells. *Nature* **2001,** *414* (6861), 338-344.
7. Li, H.; Zhou, Y.; Tu, W.; Ye, J.; Zou, Z., State-of-the-Art Progress in Diverse Heterostructured Photocatalysts toward Promoting Photocatalytic Performance. *Advanced Functional Materials* **2015,** *25* (7), 998-1013.
8. Siva Krishna, K.; Rowena, Y.; Parvathala Reddy, N.; Jennifer, W.-L.; Li, L.; Kaushal, V.; Hark Hoe, T.; Chennupati, J., CdS/TiO2 Photoanodes via Solution Ion Transfer Method for Highly Efficient Solar Hydrogen Generation. *Nano Futures* **2018,** *2* (1), 015004.
9. Kamat, P. V.; Christians, J. A., Solar Cells versus Solar Fuels: Two Different Outcomes. *The Journal of Physical Chemistry Letters* **2015,** *6* (10), 1917-1918.
10. Zhang, K.; Ma, M.; Li, P.; Wang, D. H.; Park, J. H., Water Splitting Progress in Tandem Devices: Moving Photolysis beyond Electrolysis. *Advanced Energy Materials* **2016,** *6* (15), 1600602-n/a.
11. Fountaine, K. T.; Lewerenz, H. J.; Atwater, H. A., Efficiency Limits for Photoelectrochemical Water-Splitting. *Nature Communications* **2016,** *7*.
12. Prévot, M. S.; Sivula, K., Photoelectrochemical Tandem Cells for Solar Water Splitting. *The Journal of Physical Chemistry C* **2013,** *117* (35), 17879-17893.
13. Brillet, J.; Yum, J.-H.; Cornuz, M.; Hisatomi, T.; Solarska, R.; Augustynski, J.; Graetzel, M.; Sivula, K., Highly Efficient Water Splitting by a Dual-Absorber Tandem Cell. *Nat Photon* **2012,** *6* (12), 824-828.
14. Gurudayal; Sabba, D.; Kumar, M. H.; Wong, L. H.; Barber, J.; Grätzel, M.; Mathews, N., Perovskite–Hematite Tandem Cells for Efficient Overall Solar Driven Water Splitting. *Nano letters* **2015,** *15* (6), 3833-3839.
15. Shi, X.; Zhang, K.; Shin, K.; Ma, M.; Kwon, J.; Choi, I. T.; Kim, J. K.; Kim, H. K.; Wang, D. H.; Park, J. H., Unassisted Photoelectrochemical Water Splitting beyond 5.7% Solar-to-Hydrogen Conversion Efficiency by a Wireless Monolithic Photoanode/Dye-Sensitised Solar Cell Tandem Device. *Nano Energy* **2015,** *13* (Supplement C), 182-191.
16. Abdi, F. F.; Han, L.; Smets, A. H. M.; Zeman, M.; Dam, B.; van de Krol, R., Efficient Solar Water Splitting by Enhanced Charge Separation in a Bismuth Vanadate-Silicon Tandem Photoelectrode. **2013,** *4*, 2195.

17. Shin, K.; Park, J. H., Highly Transparent Dual-Sensitized Titanium Dioxide Nanotube Arrays for Spontaneous Solar Water Splitting Tandem Configuration. *ACS Applied Materials & Interfaces* **2015,** *7* (33), 18429-18434.
18. Luo, J.; Li, Z.; Nishiwaki, S.; Schreier, M.; Mayer, M. T.; Cendula, P.; Lee, Y. H.; Fu, K.; Cao, A.; Nazeeruddin, M. K.; Romanyuk, Y. E.; Buecheler, S.; Tilley, S. D.; Wong, L. H.; Tiwari, A. N.; Grätzel, M., Targeting Ideal Dual-Absorber Tandem Water Splitting Using Perovskite Photovoltaics and CuInxGa1-xSe2 Photocathodes. *Advanced Energy Materials* **2015,** *5* (24), 1501520-n/a.
19. Kim, J. H.; Jo, Y.; Kim, J. H.; Jang, J. W.; Kang, H. J.; Lee, Y. H.; Kim, D. S.; Jun, Y.; Lee, J. S., Wireless Solar Water Splitting Device with Robust Cobalt-Catalyzed, Dual-Doped BiVO4 Photoanode and Perovskite Solar Cell in Tandem: A Dual Absorber Artificial Leaf. *ACS nano* **2015,** *9* (12), 11820-11829.
20. Qiu, Y.; Liu, W.; Chen, W.; Chen, W.; Zhou, G.; Hsu, P.-C.; Zhang, R.; Liang, Z.; Fan, S.; Zhang, Y.; Cui, Y., Efficient Solar-Driven Water Splitting by Nanocone BiVO4/Perovskite Tandem Cells. *Science Advances* **2016,** *2* (6).
21. Xiao, S.; Hu, C.; Lin, H.; Meng, X.; Bai, Y.; Zhang, T.; Yang, Y.; Qu, Y.; Yan, K.; Xu, J.; Qiu, Y.; Yang, S., Integration of Inverse Nanocone Array based Bismuth Vanadate Photoanodes and Bandgap-tunable Perovskite Solar Cells for Efficient Self-Powered Solar Water Splitting. *Journal of Materials Chemistry A* **2017,** *5* (36), 19091-19097.
22. Luo, J.; Im, J.-H.; Mayer, M. T.; Schreier, M.; Nazeeruddin, M. K.; Park, N.-G.; Tilley, S. D.; Fan, H. J.; Grätzel, M., Water Photolysis at 12.3% Efficiency via Perovskite Photovoltaics and Earth-Abundant Catalysts. *Science* **2014,** *345* (6204), 1593-1596.
23. Kamat, P. V., Hybrid Perovskites for Multijunction Tandem Solar Cells and Solar Fuels. A Virtual Issue. *ACS Energy Letters* **2018,** *3* (1), 28-29.
24. Yang, W. S.; Park, B.-W.; Jung, E. H.; Jeon, N. J.; Kim, Y. C.; Lee, D. U.; Shin, S. S.; Seo, J.; Kim, E. K.; Noh, J. H.; Seok, S. I., Iodide Management in Formamidinium-Lead-Halide–based Perovskite Layers for Efficient Solar Cells. *Science* **2017,** *356* (6345), 1376-1379.
25. Zhang, X.; Zhang, B.; Cao, K.; Brillet, J.; Chen, J.; Wang, M.; Shen, Y., A Perovskite Solar Cell-TiO2/BiVO4 Photoelectrochemical System for Direct Solar Water Splitting. *Journal of Materials Chemistry A* **2015,** *3* (43), 21630-21636.
26. Iwase, A.; Kudo, A.; Numata, Y.; Ikegami, M.; Miyasaka, T.; Ichikawa, N.; Kato, M.; Hashimoto, H.; Inoue, H.; Ishitani, O.; Tamiaki, H., Solar Water Splitting Utilizing a SiC Photocathode, a BiVO4 Photoanode, and a Perovskite Solar Cell. *ChemSusChem*, n/a-n/a.
27. Dias, P.; Schreier, M.; Tilley, S. D.; Luo, J.; Azevedo, J.; Andrade, L.; Bi, D.; Hagfeldt, A.; Mendes, A.; Grätzel, M.; Mayer, M. T., Transparent Cuprous Oxide Photocathode Enabling a Stacked Tandem Cell for Unbiased Water Splitting. *Advanced Energy Materials* **2015,** *5* (24), 1501537-n/a.
28. Karuturi, S. K.; Liu, L.; Su, L. T.; Zhao, Y.; Fan, H. J.; Ge, X.; He, S.; Yoong, A. T. I., Kinetics of Stop-Flow Atomic Layer Deposition for High Aspect Ratio Template Filling through Photonic Band Gap Measurements. *The Journal of Physical Chemistry C* **2010,** *114* (35), 14843-14848.
29. Luo, J. S.; Karuturi, S. K.; Liu, L.; Su, L. T.; Tok, A. I. Y.; Fan, H. J., Homogeneous Photosensitization of Complex TiO2 Nanostructures for Efficient Solar Energy Conversion. *Scientific Reports* **2012,** *2*, 451.
30. Lee, Y.-L.; Chi, C.-F.; Liau, S.-Y., CdS/CdSe Co-Sensitized TiO2 Photoelectrode for Efficient Hydrogen Generation in a Photoelectrochemical Cell. *Chemistry of Materials* **2010,** *22* (3), 922-927.
31. Yu, J.; Gong, C.; Wu, Z.; Wu, Y.; Xiao, W.; Su, Y.; Sun, L.; Lin, C., Efficient Visible Light-Induced Photoelectrocatalytic Hydrogen Production using CdS Sensitized TiO2 Nanorods on TiO2 Nanotube Arrays. *Journal of Materials Chemistry A* **2015,** *3* (44), 22218-22226.
32. Shin, K.; Seok, S. i.; Im, S. H.; Park, J. H., CdS or CdSe Decorated TiO2 Nanotube Arrays from Spray Pyrolysis Deposition: Use in Photoelectrochemical Cells. *Chemical Communications* **2010,** *46* (14), 2385-2387.

33. Shen, H.; Wu, Y.; Peng, J.; Duong, T.; Fu, X.; Barugkin, C.; White, T. P.; Weber, K.; Catchpole, K. R., Improved Reproducibility for Perovskite Solar Cells with 1 cm2 Active Area by a Modified Two-Step Process. *ACS applied materials & interfaces* **2017,** *9* (7), 5974-5981.
34. Liu, M.; Li, X.; Karuturi, S. K.; Tok, A. I. Y.; Fan, H. J., Atomic Layer Deposition for Nanofabrication and Interface Engineering. *Nanoscale* **2012,** *4* (5), 1522-1528.
35. George, S. M., Atomic Layer Deposition: An Overview. *Chemical Reviews* **2010,** *110* (1), 111-131.
36. Sun, W.-T.; Yu, Y.; Pan, H.-Y.; Gao, X.-F.; Chen, Q.; Peng, L.-M., CdS Quantum Dots Sensitized TiO2 Nanotube-Array Photoelectrodes. *Journal of the American Chemical Society* **2008,** *130* (4), 1124-1125.
37. Saliba, M.; Matsui, T.; Seo, J.-Y.; Domanski, K.; Correa-Baena, J.-P.; Nazeeruddin, M. K.; Zakeeruddin, S. M.; Tress, W.; Abate, A.; Hagfeldt, A.; Gratzel, M., Cesium-containing Triple Cation Perovskite Solar Cells: Improved Stability, Reproducibility and High Efficiency. *Energy & Environmental Science* **2016,** *9* (6), 1989-1997.
38. Tress, W.; Marinova, N.; Moehl, T.; Zakeeruddin, S. M.; Nazeeruddin, M. K.; Grätzel, M., Understanding the Rate-Dependent JV Hysteresis, Slow Time Component, and Aging in CH3NH3PbI3 Perovskite Solar Cells: The Role of a Compensated Electric Field. *Energy & Environmental Science* **2015**.
39. Jacobs, D. A.; Wu, Y.; Shen, H.; Barugkin, C.; Beck, F. J.; White, T. P.; Weber, K.; Catchpole, K. R., Hysteresis Phenomena in Perovskite Solar Cells: The Many and Varied Effects of Ionic Accumulation. *Physical Chemistry Chemical Physics* **2017,** *19* (4), 3094-3103.
40. Rabinovich, E.; Hodes, G., Effective Bandgap Lowering of CdS Deposited by Successive Ionic Layer Adsorption and Reaction. *The Journal of Physical Chemistry C* **2013,** *117* (4), 1611-1620.
41. Wu, Y.; Shen, H.; Walter, D.; Jacobs, D.; Duong, T.; Peng, J.; Jiang, L.; Cheng, Y.-B.; Weber, K., On the Origin of Hysteresis in Perovskite Solar Cells. *Advanced Functional Materials* **2016,** *26* (37), 6807-6813.
42. Heping, S.; Jacobs, D.; Wu, Y.; Duong, T.; Peng, J.; Wen, X.; Karuturi, S. K., Inverted Hysteresis in CH3NH3PbI3 Solar Cells: Role of Stoichiometry and Band Alignment. *The Journal of Physical Chemistry Letters* **2017,** *8* (12), 2672-2680.
43. Ai, G.; Li, H.; Liu, S.; Mo, R.; Zhong, J., Solar Water Splitting by TiO2/CdS/Co–Pi Nanowire Array Photoanode Enhanced with Co–Pi as Hole Transfer Relay and CdS as Light Absorber. *Advanced Functional Materials* **2015,** *25* (35), 5706-5713.
44. Yang, H. B.; Miao, J.; Hung, S.-F.; Huo, F.; Chen, H. M.; Liu, B., Stable Quantum Dot Photoelectrolysis Cell for Unassisted Visible Light Solar Water Splitting. *ACS Nano* **2014,** *8* (10), 10403-10413.

## Table of Contents Graphic